Article

Binding and Condensation of Plasmid DNA onto Functionalized Carbon Nanotubes: Toward the Construction of Nanotube-Based Gene Delivery Vectors

Ravi Singh, Davide Pantarotto, David McCarthy, Olivier Chaloin, Johan Hoebeke, Charalambos D. Partidos, Jean-Paul Briand, Maurizio Prato, Alberto Bianco, and Kostas Kostarelos

J. Am. Chem. Soc., **2005**, 127 (12), 4388-4396• DOI: 10.1021/ja0441561 • Publication Date (Web): 08 March 2005

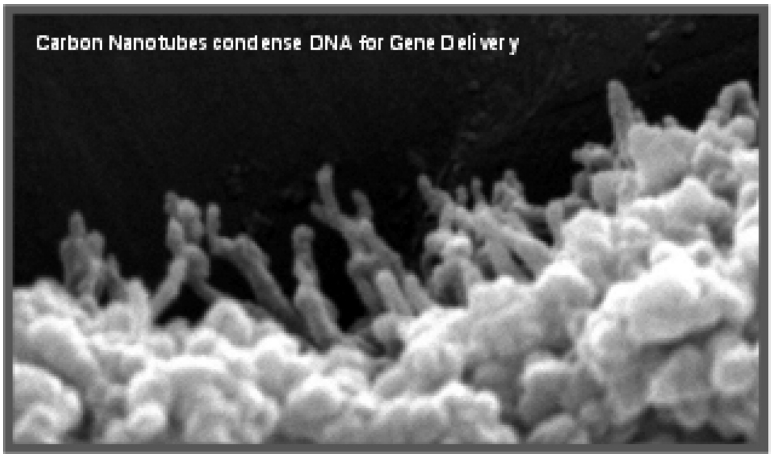

More About This Article

Additional resources and features associated with this article are available within the HTML version:

- Supporting Information
- Links to the 44 articles that cite this article, as of the time of this article download
- Access to high resolution figures
- Links to articles and content related to this article
- Copyright permission to reproduce figures and/or text from this article

View the Full Text HTML

J|A|C|S
ARTICLES
Published on Web 03/08/2005

Binding and Condensation of Plasmid DNA onto Functionalized Carbon Nanotubes: Toward the Construction of Nanotube-Based Gene Delivery Vectors

Ravi Singh,[†] Davide Pantarotto,[‡,§] David McCarthy,[||] Olivier Chaloin,[‡] Johan Hoebeke,[‡] Charalambos D. Partidos,[‡] Jean-Paul Briand,[‡] Maurizio Prato,*[,§] Alberto Bianco,*[,‡] and Kostas Kostarelos*[,†]

Contribution from the Centre for Drug Delivery Research and Electron Microscopy Unit, The School of Pharmacy, University of London, London WC1N 1AX, United Kingdom, Immunologie et Chimie Thérapeutiques, Institut de Biologie Moléculaire et Cellulaire, UPR9021 CNRS, 67084 Strasbourg, France, and Dipartimento di Scienze Farmaceutiche, Università di Trieste, 34127 Trieste, Italy

Received September 26, 2004; E-mail: kostas.kostarelos@ulsop.ac.uk; A.Bianco@ibmc.u-strasbg.fr; prato@univ.trieste.it

Abstract: Carbon nanotubes (CNTs) constitute a class of nanomaterials that possess characteristics suitable for a variety of possible applications. Their compatibility with aqueous environments has been made possible by the chemical functionalization of their surface, allowing for exploration of their interactions with biological components including mammalian cells. Functionalized CNTs (f-CNTs) are being intensively explored in advanced biotechnological applications ranging from molecular biosensors to cellular growth substrates. We have been exploring the potential of f-CNTs as delivery vehicles of biologically active molecules in view of possible biomedical applications, including vaccination and gene delivery. Recently we reported the capability of ammonium-functionalized single-walled CNTs to penetrate human and murine cells and facilitate the delivery of plasmid DNA leading to expression of marker genes. To optimize f-CNTs as gene delivery vehicles, it is essential to characterize their interactions with DNA. In the present report, we study the interactions of three types of f-CNTs, ammonium-functionalized single-walled and multiwalled carbon nanotubes (SWNT-NH_3^+; MWNT-NH_3^+), and lysine-functionalized single-walled carbon nanotubes (SWNT-Lys-NH_3^+), with plasmid DNA. Nanotube−DNA complexes were analyzed by scanning electron microscopy, surface plasmon resonance, PicoGreen dye exclusion, and agarose gel shift assay. The results indicate that all three types of cationic carbon nanotubes are able to condense DNA to varying degrees, indicating that both nanotube surface area and charge density are critical parameters that determine the interaction and electrostatic complex formation between f-CNTs with DNA. All three different f-CNT types in this study exhibited upregulation of marker gene expression over naked DNA using a mammalian (human) cell line. Differences in the levels of gene expression were correlated with the structural and biophysical data obtained for the f-CNT:DNA complexes to suggest that large surface area leading to very efficient DNA condensation is not necessary for effective gene transfer. However, it will require further investigation to determine whether the degree of binding and tight association between DNA and nanotubes is a desirable trait to increase gene expression efficiency in vitro or in vivo. This study constitutes the first thorough investigation into the physicochemical interactions between cationic functionalized carbon nanotubes and DNA toward construction of carbon nanotube-based gene transfer vector systems.

Introduction

Nanomaterials are revolutionizing a wide range of fields and applications by allowing control of materials' structure at the molecular scale. This has led to improved characteristics and functions, as well as the creation of new functional material. Significant enhancement of optical, mechanical, electrical, structural, and magnetic properties are commonly found through the use of novel nanomaterials.[1] In the biotechnology field, colloidal nanoparticle systems have been employed for a number of applications from enzyme immobilization to the development of delivery systems for anticancer agents.[2] Novel nanomaterials are expected to further impact biomedicine as advanced biosensors, diagnostics, and drug delivery systems,[3] after biocompatibility and toxicity issues have been resolved.

[†] Centre for Drug Delivery Research, The School of Pharmacy, University of London.
[‡] UPR9021 CNRS.
[§] Università di Trieste.
[||] Electron Microscopy Unit, The School of Pharmacy, University of London.

(1) Niemeyer, C. M., Mirkin, C. A., Eds. *Nanobiotechnology: Concepts, Applications and Perspectives*; Wiley-VCH: Weinheim, Germany, 2004.
(2) Moghimi, S. M.; Hunter, A. C.; Murray, J. C. *Pharmacol. Rev.* **2001**, *53*, 283−318.
(3) Zhang, S. *Nat. Biotechnol.* **2003**, *21*, 1171−1178.

10.1021/ja0441561 CCC: $30.25

One of the most exciting classes of nanomaterials is represented by the carbon nanotubes (CNTs), or "buckytubes".[4] CNTs possess extraordinary properties, including high electrical and thermal conductivity and great strength, rigidity, and are being developed for a wealth of applications, including field emission,[5] energy storage,[6] molecular electronics,[7] and atomic force microscopy (AFM).[8] CNTs have proven difficult to solubilize in aqueous solutions, limiting their use in biological applications.[9,10] However, even though exploration of the biomedical applications of carbon nanotubes is in nascent stages, it has already shown significant promise.[10,11] Such include their use as DNA[12,13] and protein biosensors[14] or ion channel blockers.[15]

One of the most commonly used strategies to render carbon nanotubes soluble in aqueous media, and therefore, potentially useful to biomedical applications, is through their surface functionalization (f-CNT).[9,16,17] Functionalization of carbon nanotubes can be achieved either by covalent or noncovalent methodologies.[9,17−19] Various biological applications for f-CNTs have been proposed such as substrates for neuronal cell growth[20] and as bioseparators and biocatalysts.[21] We previously demonstrated that peptide functionalized carbon nanotubes are capable of penetrating the mammalian plasma membrane and translocating to the cell nucleus[22] and that these nanotubes are capable of eliciting an antigen-specific neutralizing antibody response in vivo.[23] Intracellular transport of proteins bound onto carbon nanotubes has been also confirmed by Wender and Dai.[24] More recently, we reported the first case of carbon nanotube-mediated intracellular delivery of a biologically active molecule using ammonium-functionalized single-walled carbon nanotubes (SWNT-NH_3^+) complexed to plasmid DNA leading to gene expression levels up to 10-fold that of naked DNA alone.[25] These observations indicated that complex formation between f-CNTs and DNA can constitute a novel class of nonviral gene delivery systems.

Indeed, for successful gene therapy an efficient delivery system is required. This will allow the transfer and expression of the therapeutic gene in the target organ or tissue. To this end, both viral and nonviral vectors are currently in use. Although viral gene delivery achieves high levels of gene expression, it has several disadvantages that make it problematic for human use. In particular, viral vectors can be immunogenic, or induce inflammation that render transgene expression transient, or can have oncogenic effects.[26] Nonviral vectors might be more desirable since they can overcome some of these concerns. In addition, because these vectors are typically assembled in cell-free systems from well-defined components, they can have significant manufacturing and safety advantages over viral vectors. However, improvements of nonviral vectors to achieve therapeutically relevant levels of gene expression are still needed.

The use of cationic molecules such as various synthetic lipids, polylysine, protamine sulfate, and cationic dendrimers to condense DNA and form complexes able to enhance the efficiency of gene transfer in vitro and in vivo is well-documented.[27,28] Such DNA condensates are commonly of a spherical morphology, while the molecular interactions between DNA and the cationic component greatly determine a number of biological processes responsible for efficient gene expression. These include enhancement of cell membrane interactions due to electrostatic forces, increased cellular uptake by endocytosis, and improved trafficking to the nucleus. To optimize f-CNTs as gene delivery vehicles, it is essential to characterize their interactions with DNA. In the present report, we study the interactions of three types of f-CNTs, ammonium-functionalized single-walled and multiwalled carbon nanotubes (SWNT-NH_3^+ (**1**), MWNT-NH_3^+ (**2**)) and lysine-functionalized single-walled carbon nanotubes (SWNT-Lys-NH_3^+ (**3**)) (Figure 1), with plasmid DNA. Nanotube−DNA complexes were analyzed by scanning electron microscopy (SEM), surface plasmon resonance (SPR), PicoGreen dye exclusion, and agarose gel shift

(4) (a) Iijima, S. *Nature* **1991**, *354*, 56−58; (b) Special Issue on Carbon Nanotubes. *Acc. Chem. Res.* **2002**, *35*, 997−1113.
(5) (a) Milne, W. I.; Teo, K. B. K.; Amaratunga, G. A. J.; Legagneux, P.; Gangloff, L.; Schnell, J. P.; Semet, V.; Binh, V. T.; Groening, O. *J. Mater. Chem.* **2004**, *14*, 933−943. (b) Park, N.; Han, S.; Ihm, J. *J. Nanosci. Nanotechnol.* **2003**, *3*, 179−183.
(6) (a) Hirscher, M.; Becher, M. *J. Nanosci. Nanotechnol.* **2003**, *3*, 3−17. (b) Chen, G.; Bandow, S.; Margine, E. R.; Nisoli, C.; Kolmogorov, A. N.; Crespi, V. H.; Gupta, R.; Sumanasekera, G. U.; Iijima, S.; Eklund, P. C. *Phys. Rev. Lett.* **2003**, *90*, 2574031−2574034.
(7) (a) Weisman, R. B. *Nat. Mater.* **2003**, *2*, 569−570. (b) Service, R. F. *Science* **2003**, *302*, 1310. (c) Javey, A.; Guo, J.; Wang, Q.; Lundstrom, M.; Dai, H. *Nature* **2003**, *424*, 654−657.
(8) (a) Schnitzler, G. R.; Cheung, C. L.; Hafner, J. H.; Saurin, A. J.; Kingston, R. E.; Lieber, C. M. *Mol. Cell. Biol.* **2001**, *21*, 8504−8511. (b) Hafner, J. H.; Cheung, C. L.; Woolley, A. T.; Lieber, C. M. *Prog. Biophys. Mol. Biol.* **2001**, *77*, 73−110.
(9) Tasis, D.; Tagmatarchis, N.; Georgakilas, V.; Prato, M. *Chem. Eur. J.* **2003**, *9*, 4000−4008.
(10) Lin, Y.; Taylor, S.; Li, H. P.; Fernando, K. A. S.; Qu, L. W.; Wang, W.; Gu, L. R.; Zhou, B.; Sun, Y. P. *J. Mater. Chem.* **2004**, *14*, 527−541.
(11) (a) Bradbury, J. *Lancet* **2003**, *362*, 1984−1985. (b) Bianco, A.; Prato, M. *Adv. Mater.* **2003**, *15*, 1765−1768.
(12) (a) Baker, S. E.; Cai, W.; Lasseter, T. L.; Weidkamp, K. P.; Hamers, R. J. *Nano Lett.* **2002**, *2*, 1413−1417. (b) Nguyen, C. V.; Delzeit, L.; Cassell, A. M.; Li, J.; Han, J.; Meyyappan, M. *Nano Lett.* **2002**, *2*, 1079−1081. (c) Cai, H.; Cao, X.; Jiang, Y.; He, P.; Fang, Y. *Anal. Bioanal. Chem.* **2003**, *375*, 287−293.
(13) Williams, K. A.; Veenhuizen, P. T.; de la Torre, B. G.; Eritja, R.; Dekker, C. *Nature* **2002**, *420*, 761.
(14) (a) Gooding, J. J.; Wibowo, R.; Liu, J. Q.; Yang, W. R.; Losic, D.; Orbons, S.; Mearns, F. J.; Shapter, J. G.; Hibbert, D. B. *J. Am. Chem. Soc.* **2003**, *125*, 9006−9007. (b) Wang, J.; Liu, G.; Jan, M. R. *J. Am. Chem. Soc.* **2004**, *126*, 3010−3011. (c) Chen, R. J.; Bangsaruntip, S.; Drouvalakis, K. A.; Kam, N. W.; Shim, M.; Li, Y.; Kim, W.; Utz, P. J.; Dai, H. *Proc. Natl. Acad. Sci. U.S.A.* **2003**, *100*, 4984−4989.
(15) Park, K. H.; Chhowalla, M.; Iqbal, Z.; Sesti, F. *J. Biol. Chem.* **2003**, *278*, 50212−50216.
(16) Wong, S. S.; Joselevich, E.; Woolley, A. T.; Cheung, C. L.; Lieber, C. M. *Nature* **1998**, *394*, 52−55.
(17) (a) Hirsch, A. *Angew. Chem., Int. Ed.* **2002**, *41*, 1853−1859. (b) Dyke, C. A.; Tour, J. M. *Chem. Eur. J.* **2004**, *10*, 813−817.
(18) (a) Chen, R. J.; Zhang, Y.; Wang, D.; Dai, H. *J. Am. Chem. Soc.* **2001**, *123*, 3838−3839. (b) Star, A.; Steuerman, D.; Heath, J. R.; Stoddard, J. F. *Angew. Chem., Int. Ed.* **2002**, *41*, 2508−2512. (c) Richard, C.; Balavoine, F.; Schultz, P.; Ebbesen, T. W.; Mioskowski, C. *Science* **2003**, *300*, 775−778. (d) Dieckmann, G. R.; Dalton, A. B.; Johnson, P. A.; Razal, J.; Chen, J.; Giordano, G. M.; Munoz, E.; Musselman, I. H.; Baughman, R. H.; Draper, R. K. *J. Am. Chem. Soc.* **2003**, *125*, 1770−1777.
(19) Zheng, M.; Jagota, A.; Semke, E. D.; Diner, B. A.; McLean, R. S.; Lustig, S. R.; Richardson, R. E.; Tassi, N. G. *Nat. Mater.* **2003**, *2*, 338−342.
(20) (a) Hui, H.; Yingchun, N.; Vedrana, M.; Haddon, R. C.; Parpura, V. *Nano Lett.* **2004**, *4*, 507−511. (b) Mattson, M. P.; Haddon, R. C.; Rao, A. M. *J. Mol. Neurosci.* **2000**, *14*, 175−182.
(21) Mitchell, D. T.; Lee, S. B.; Trofin, L.; Li, N.; Nevanen, T. K.; Soderlund, H.; Martin, C. R. *J. Am. Chem. Soc.* **2002**, *124*, 11864−11865.
(22) Pantarotto, D.; Briand, J. P.; Prato, M.; Bianco, A. *Chem. Commun.* **2004**, *1*, 16−17.
(23) Pantarotto, D.; Partidos, C. D.; Hoebeke, J.; Brown, F.; Kramer, E.; Briand, J. P.; Muller, S.; Prato, M.; Bianco, A. *Chem. Biol.* **2003**, *10*, 961−966.
(24) Shi, K. N. W.; Jessop, T. C.; Wender, P. A.; Dai, H. *J. Am. Chem. Soc.* **2004**, *126*, 6850−6851.
(25) Pantarotto, D.; Singh, R.; McCarthy, D.; Erhard, M.; Briand, J. P.; Prato, M.; Kostarelos, K.; Bianco, A. *Angew. Chem., Int. Ed.* **2004**, *43*, 5242−5246.
(26) Thomas, C.; Ehrhardt, A.; Kay, M. *Nat. Rev. Genet.* **2003**, *4*, 346−358.
(27) (a) Lasic, D. D.; Strey, H.; Stuart, M. C. A.; Podgornik, R.; Frederik, P. M. *J. Am. Chem. Soc.* **1997**, *119*, 832−833. (b) Choi, J. S.; Joo, D. K.; Kim, C. H.; Kim, K.; Park, J. S. *J. Am. Chem. Soc.* **2000**, *122*, 474−480. (c) Matulis, D.; Rouzina, I.; Bloomfield, V. A. *J. Am. Chem. Soc.* **2002**, *124*, 7331−7342. (d) Zinselmeyer, B. H.; Mackay, S. P.; Schatzlein, A. G.; Uchegbu, I. F. *Pharm. Res.* **2002**, *19*, 960−967. (e) Sorgi, F. L.; Bhattacharya, S.; Huang, L. *Gene Ther.* **1997**, *4*, 961−968.
(28) Parker, A. L.; Oupicky, D.; Dash, P. R.; Seymour, L. W. *Anal. Biochem.* **2002**, *302*, 75−80.

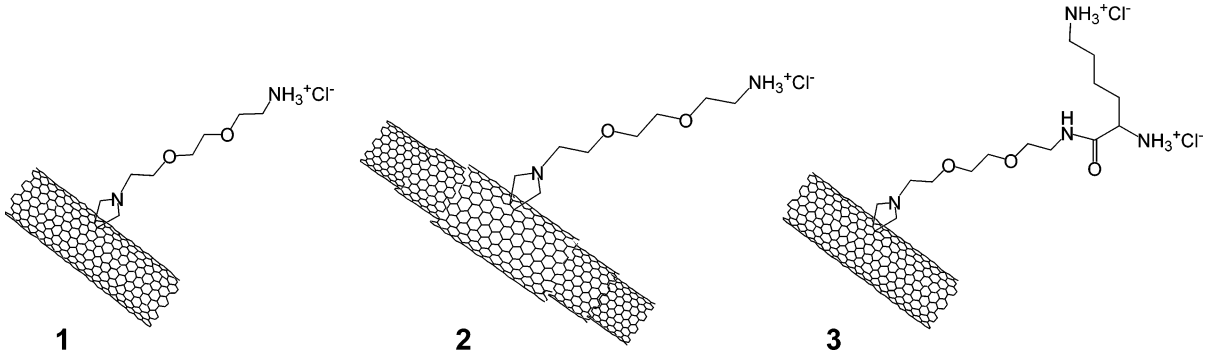

Figure 1. Molecular structures of ammonium-functionalized carbon nanotubes.

assay. Additionally, an in vitro transfection study was conducted to determine if the various types of funtionalized nanotubes were capable of acting as gene transfer agents. The results indicate that all three types of cationic carbon nanotubes are able to condense DNA to varying degrees and that they all can successfully deliver plasmid DNA to cells, leading to gene expression. To our knowledge, this study constitutes the first thorough investigation into the physicochemical interactions between cationic functionalized carbon nanotubes and DNA toward construction of novel, carbon nanotube-based gene-transfer vector systems.

Materials and Methods

General Procedure. SWNT-NH_3^+ (**1**), MWNT-NH_3^+ (**2**), and SWNT-Lys-NH_3^+ (**3**; Figure 1) were prepared as previously described.[23,29] Ammonium-functionalized, single-walled (**1**) and multi-walled carbon nanotubes (**2**) were solubilized in deionized water at a concentration of 6 and 6.6 mg/mL, respectively. Lysine-functionalized single-walled carbon nanotubes (**3**) were dissolved in deionized water at a concentration of 3.3 mg/mL. All solutions were sonicated for 1 min at room temperature in a bath sonicator (80 W, EMscope Laboratories, U.K.) and then stored at 4 °C until needed. Prior to use, nanotube solutions were briefly sonicated once again. The plasmid used for these studies was pCMV−Bgal (BD-Clontech, U.K.), a 7.2 kb, eukaryotic expression vector. A gigaprep of highly purified supercoiled DNA was prepared by Bayou Biolabs (LA). A stock solution was prepared in deionized water at a concentration of 1 mg/mL. Aliquots were stored frozen at −80 °C until use.

f-CNT:DNA Complexes. To prepare the carbon nanotube:DNA complexes, the appropriate volume of each type of nanotube was diluted to a total volume of 200 μL in deionized water and then split into four 50 μL aliquots for each concentration of f-CNT. Depending on the type of nanotube and charge ratio needed, f-CNT concentrations ranged from 16.5 to 300 μg/mL. An equal volume of a 5 μg/mL DNA solution was then added to three of the f-CNT aliquots and then mixed by rapidly pipetting 10 times, yielding a final DNA concentration of 250 ng/mL. A 50 μL aliquot of deionized water was added to the fourth f-CNT aliquot of each group as a nanotube-only control. Complexes were allowed to form for 30 min at room temperature prior to use. This process was repeated for each charge ratio tested, yielding three samples per condition plus a nanotube-only sample at the corresponding concentration.

Scanning Electron Microscopy. SEM was used to image SWNT-NH_3^+ (**1**) and MWNT-NH_3^+ (**2**) complexed with the plasmid DNA. Imaging was carried out by placing a 30 μL drop of the 6:1 (CNT:DNA) charge ratio complex samples or an equivalent concentration of nanotubes alone onto the SEM stub and allowed to dry at room temperature prior to gold coating. This was performed in an Emitech K550 sputter coater for 2 min at 20 mA. Imaging was carried out under a FEI/Philips XL 30 scanning electron microscope (Eindhoven, The Netherlands) at an accelerating voltage between 20 and 25 kV (see also on each image). Images were captured and saved digitally.

Surface Plasmon Resonance. The BIAcore 3000 system, sensor chip CM5, surfactant P20, amine coupling kit containing *N*-hydroxysuccinimide (NHS), and *N*-ethyl-*N*′-(dimethylaminopropyl)carbodiimide (EDC) were from BIAcore (Uppsala, Sweden). All biosensor assays were performed with HBS as running buffer (20 mM HEPES, 20 mM sodium acetate, 140 mM potassium acetate, 3 mM magnesium acetate, 0.02% surfactant P20, pH 7.3). Immobilization of nanotubes was performed by injecting 35 μL of nanotubes (100 μg/mL in acetate buffer, pH 4.0) onto the surface of a sensor chip CM5 activated with EDC/NHS. This was followed by 20 μL of ethanolamine hydrochloride, pH 8.5, to saturate the free activated sites of the matrix. A 100 mM H_3PO_4 solution was used to remove nanotubes noncovalently immobilized on the chip. All the binding experiments were carried out at 25 °C with a constant flow rate of 30 μL/mn. pCMV−BGal was dissolved in the running buffer. Different concentrations of plasmid (6.3−100 μg/mL) were injected for 90 s, followed by a dissociation phase of 2 min. In all experiments, the sensor chips were regenerated with 15 μL of 3 M $MgCl_2$. The kinetic parameters were calculated using the BIAeval 3.1 software. Analysis was performed using the simple Langmuir binding model. The specific binding profiles were obtained after subtracting the response signal from the channel control. The fitting to each model was judged by the χ^2 value and the randomness of the residue distribution compared to the theoretical model.

PicoGreen Assay for f-CNT:DNA Complexes. The degree of DNA accessibility following complexation with f-CNTs was assessed by the double-stranded-DNA-binding reagent PicoGreen (Molecular Probes, OR). Briefly, the carbon nanotube:DNA complexes were diluted 10× with deionized water to yield a final DNA concentration of 250 ng/mL, and then 100 μL of sample was added to triplicate wells of a CoStar 96-well special optics black plate (Corning, NY). Because the plasmid used for this study, pCMV−Bgal, primarily is in a supercoiled state, a standard curve ranging from 1000 to 31.25 ng/mL was generated using this plasmid rather than the control included with the assay kit. A 100 μL aliquot of PicoGreen reagent in 2× TE buffer (20 mM Tris/HCl/2 mM EDTA, pH 7.5) was added in each well, and the plate was incubated in the dark for 3 min and then measured at excitation and emission wavelengths of 485 and 530 nm, respectively, using a Wallac Victor^2 (Wallac, U.K.) multiwell plate reader. Because the carbon nanotubes alone autofluoresce at the measured wavelength, a second standard curve of carbon nanotubes alone was generated to quantify the background fluorescence. This was then subtracted from each sample. Percent free DNA was determined by dividing the background-corrected PicoGreen counts of each complex by the background-corrected measurement of 250 ng/mL of pBgal alone, representing

(29) (a) Pantarotto, D.; Partidos, C. D.; Graff, R.; Hoebeke, J.; Briand, J. P.; Prato, M.; Bianco, A. *J. Am. Chem. Soc.* **2003**, *125*, 6160−6164. (b) Georgakilas, V.; Tagmatarchis, N.; Pantarotto, D.; Bianco, A.; Briand, J. P.; Prato, M. *Chem. Commun.* **2002**, *24*, 3050−3051.

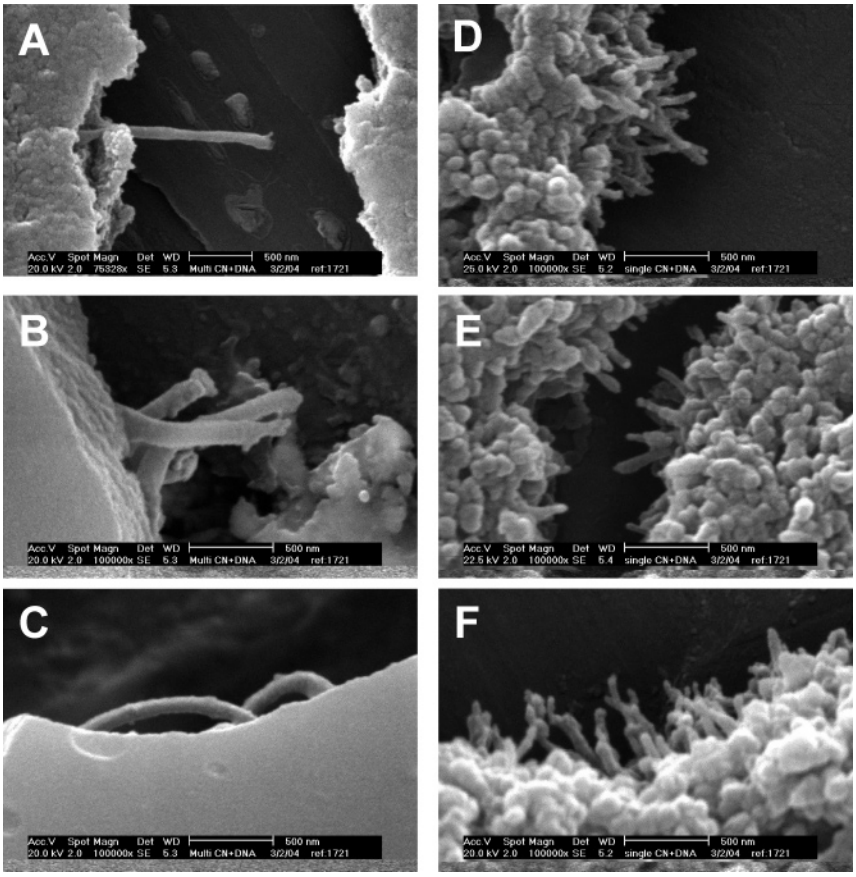

Figure 2. SEM images of carbon nanotube:DNA complexes formed at a 6:1 charge ratio: (A−C) MWNT-NH_3^+:DNA; (D−F) SWNT-NH_3^+:DNA.

Table 1. Different Types of f-CNTs Used for the Complex Formation with Plasmid DNA and SPR Physicochemical Parameters[a]

	f-CNT	cationic charge loading (mmol/g)	RU after EDC/NHS	RU after H_3PO_4	RU(max)	k_a (M^{-1} s^{-1})	k_d (s^{-1})	K_a (M^{-1})
1	SWNT-NH_3^+	0.55	4720	3038				
2	MWNT-NH_3^+	0.90	1954	1951	53.4	2.03×10^5	8.59×10^{-3}	2.36×10^7
3	SWNT-Lys-NH_3^+	0.92	6564	4369	23.1	5.54×10^5	1.24×10^{-3}	4.45×10^8

[a] Loading, number of amino functions available for the complexation; RU, SPR response expressed as resonance units (1 RU = 1 pg/mm^2 of analyte); k_a and k_d, association and dissociation rate constants; K_a, equilibrium association constant.

100% free DNA. Data are expressed as the mean of three samples, plus or minus standard deviation.

Electrophoretic Motility Shift Assay. A 0.2 μg amount of DNA (pBgal) complexed to the three types of carbon nanotubes at different charge ratios, or 0.2 μg of free DNA as a control, was added to a 1% agarose gel in TAE buffer containing ethidium bromide. The gel was run for 2 h at 90 V and then photographed under UV light using a UVP gel documentation system (Upland, CA). Each sample was run in duplicate.

Gene-Transfer Study. A549 cells (ATCC, Middlesex, U.K.) were grown in DMEM containing 10% FBS and 1% penicillin/streptomycin (all from Invitrogen/Gibco, Paisley, U.K.) until just confluent in 96-well plates. Complexes were formed by diluting 0.75 μg of pCMV−Bgal in serum-free DMEM and then by diluting the appropriate amount of **1**, **2**, or **3** in 75 μL of serum-free DMEM to yield the indicated charge ratios with 0.75 μg DNA. The DNA solution was mixed with f-CNT by rapid pipetting and allowed to stabilize for 30 min. The complete media were removed from the A549 cells and replaced with 150 μL of the various f-CNT:DNA complexes. Cells treated with media alone, or media containing 0.75 μg of DNA, were used as control. Cells were incubated with the complexes for 90 min at 37 °C, and then the transfection medium was removed and replaced with complete medium. Cells were left for 48 h, washed one time in PBS, lysed, and analyzed for β-galactosidase expression using the Tropix Galactolight Plus Kit (Applied Biosystems, CA) and a Lumat LB 9507 luminometer (Berthold Technologies, Bad Wildbad, Germany). Data are expressed as the mean of triplicate samples after subtraction of the DNA only group, plus/minus the standard deviation of the mean.

Results

To visualize the complexes formed following the interaction of f-CNT with plasmid DNA, we analyzed both **1** and **2** in the absence (Figure S1 of the Supporting Information) and presence (Figure 2) of the β-gal-expressing plasmid by SEM.

Our earlier observations demonstrated that **1** at a concentration of 180 μg/mL in aqueous solution complexed to plasmid DNA at a concentration of 5 μg/mL (yielding a 6:1 charge ratio) produced peak levels of gene expression in vitro.[25] In the present study we used the same conditions to examine the physical and morphological characteristics of the resulting complexes by SEM. MWNT-NH_3^+, due to differences in the loading of the available functional amino group (Table 1), were instead solubilized at a concentration of 99 μg/mL to yield an equivalent charge ratio when complexed to the same DNA concentration. The exact amount of the positive charges on the external walls of the different CNTs was calculated using the quantitative

Kaiser test.[29] However, when carbon nanotube:DNA complexes were formed in aqueous solution at a 6:1 charge ratio, very clear images of aggregated structures were observed throughout the SEM sample grids (Figure 2).

MWNT-NH_3^+:DNA complexes formed aggregates larger than 4 μm and possessed a planar lattice structure. DNA condensates form a concretelike planar structure with nanotubes buried within (Figure 2A−C). The DNA appears much more tightly packed, without well-defined edges separating the concretelike block. Interestingly, SEM images of the SWNT-NH_3^+:DNA complexes presented different structural features, as evidenced by the formation of almost discrete aggregate particles of 1−4 μm in diameter around the f-SWNT (Figure 2D−F). In this case the single-walled carbon nanotubes seemed to form a parallel lattice, with spherelike DNA bundles interlocking the individual tubes, while their ends can be seen extending from the edges of the complex. The SWNT-NH_3^+:DNA complexes were characterized by well-defined, spherical structures rather than the concretelike lattice observed in the case of MWNT-NH_3^+:DNA, which we believe is due to different structures attained by the condensed plasmid DNA around the cationic nanotubes. This difference may be ascribed to both the greater cationic charge density on the surface of the MWNT-NH_3^+ and the increased surface area, which allow the DNA to associate more closely with the nanotubes themselves.

In an attempt to quantify the affinity between the functionalized carbon nanotubes and plasmid DNA, we measured their interactions by SPR.[30] For this study, we also introduced a second type of f-CNT, in which the amino group of **1** was coupled to a lysine residue (Figure 1). We immobilized the nanotubes (**1**−**3**) onto the sensor chip by forming a stable amide bond between the NH_2 on the tubes and the carboxylic functions on the chip's gold surface, activated in turn with carbodiimide and *N*-hydroxysuccinimide (Table 1). This first step was followed by an acidic washing treatment to remove all reagents and excess of carbon nanotubes. The covalent immobilization of the nanotubes was demonstrated by a clear increase in the sensorgram response (Table 1).

In the case of both SWNT-NH_3^+ and SWNT-Lys-NH_3^+ (**1** and **3**), the amount of fixed tubes was significantly reduced after extensive washings with 100 mM phosphoric acid. This could be due to a nonspecific binding of a certain amount of nanotubes onto the sensor chip. The acid treatment had no effect on **2**, since no significant decrease of the resonance units (RU) was detected (Table 1). To better characterize the functionalization of the sensor chip with the nanotubes, we carried out SEM analysis of the sensor chip. Using this technique, we were able to visualize the nanotubes covalently linked to the chip's surface. Figure 3 clearly shows the SEM image of **2** on top of the carboxymethylated dextran layer that coats the sensor chip surface. The tubes range in diameter between 20 and 70 nm, and they are present as single entities. It is instead more difficult to evaluate their length distribution since they are deeply embedded into the matrix, at least partly. A similar characterization by SEM was not possible for the single-walled carbon nanotubes due to their much smaller diameter.

After immobilization of the different tubes onto the sensor chip, their interaction with the plasmid DNA, pCMV−Bgal, was examined. The plasmid was used at different concentrations

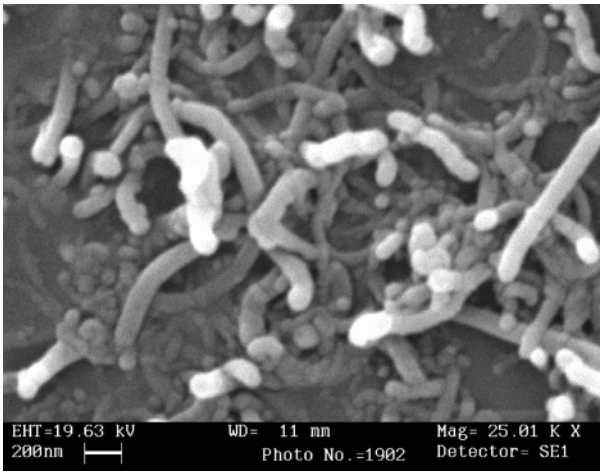

Figure 3. SEM image of the sensor chip functionalized with MWNT-NH_3^+ (**2**).

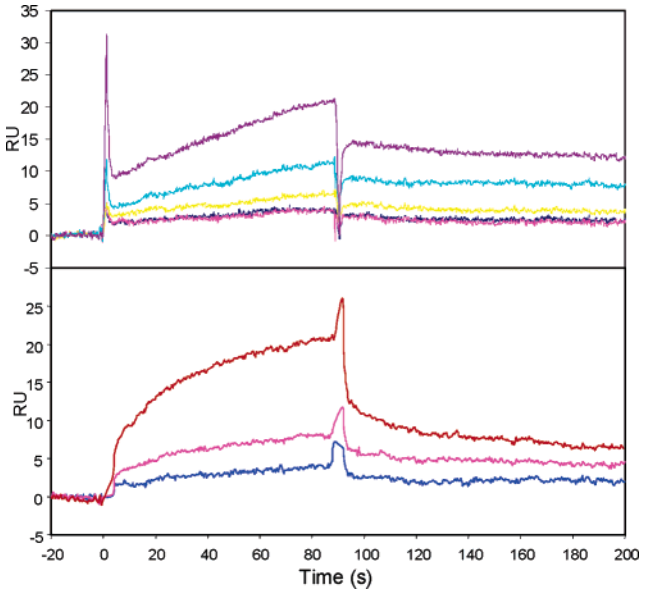

Figure 4. Sensorgrams of the interaction of the plasmid DNA with f-CNT. Top: Sensorgrams of the binding of plasmid to SWNT-Lys-NH_3^+ (**3**) by increasing the concentration of the plasmid at each run [6.3 (magenta), 12.6 (blue), 25.2 (yellow), 50 (cyan), and 100 μg/mL (violet)]. Bottom: sensorgrams of the binding of plasmid DNA to MWNT-NH_3^+ (**2**) by increasing the concentration of the plasmid at each run [25.2 (light blue), 50 (magenta), and 100 μg/mL (red)].

in the injected buffer (6.3−100 μg/mL). For each concentration, the association and dissociation curves were fitted separately using a simple Langmuir model. We were not able to detect a clear increase of the RU signal in the case of **1**. The lack of interaction can be attributed to a reduced accessibility of the positive charges available on the side wall of the tubes for the formation of complexes with the plasmid DNA. The sensorgram data for the association of the plasmid with **3** and **2** are summarized in Figure 4. Analysis of the fitting parameters enabled us to calculate an apparent equilibrium association constant of 4.45×10^8 and 2.36×10^7 M^{-1} for **3** and **2**, respectively.

SPR allows detection of complexes in the fluid phase up to 100 nm above the gold surface. If we hypothesize that the overall interaction between the immobilized carbon nanotubes and the plasmid DNA can be generally represented by those interactions detected within the signal-sensitive area above the

(30) Baird, C. L.; Myszka, D. G. *J. Mol. Recognit.* **2001**, *14*, 261−268.

gold surface (100 nm thickness), it is possible to calculate the positive:negative charge ratio between the two participating components. Simple conversion of RU values (1 RU = 1 pg/mm^2) indicates charge ratios of 62.5:1 and 11.5:1 (±) for the SWNT-Lys-NH_3^+:DNA and the MWNT-NH_3^+:DNA complexes, respectively. We have to underline that these values are approximations of the real interactions taking place, since we assumed that all amino groups on the tubes are available for complexation with the DNA. Nevertheless, this calculation indicates that MWNT-NH_3^+ are able to condense a larger amount of DNA in comparison to SWNT-Lys-NH_3^+. The difference is certainly due to the relative dimensions of the two types of nanotubes, because the charge density is almost the same in both systems. The MWNTs offer a higher available surface for interaction with the DNA. From the SPR study, we can conclude that the f-CNTs have a strong affinity for the plasmid DNA, forming a supramolecular complex which is stabilized by strong ionic interactions. The electrostatic interaction is fully reversible as confirmed by the complete dissociation of plasmid during the regeneration process of the sensor chip with magnesium chloride. This treatment brings back the RU values to those obtained after washing the sensor chip with phosphoric acid (see Table 1).

Since we were unable to measure the interaction of **1** and DNA by SPR, we also used an alternative technique to study the f-CNT:DNA complexes. The PicoGreen dye exclusion assay can be used to evaluate the degree of DNA compaction by the nanotubes in solution. PicoGreen fluorescence increases approximately 1000-fold upon intercalation between dsDNA base pairs. When DNA is condensed, the dye is prevented from interacting with it;[31] thus, a decrease in fluorescence is observed when condensed DNA is compared to an equal concentration of free DNA. The assay is slightly complicated in the case of f-CNT:DNA complexes due to the fact that the nanotubes autofluoresce under the conditions used to measure PicoGreen fluorescence (Figure S2A of the Supporting Information). It is therefore necessary to run not only a standard curve of DNA, but also a standard curve for each type of f-CNT alone to allow for correction of the background fluorescence (Figure S2B of the Supporting Information).

We assessed the interaction of all three types of f-CNTs described in this study with DNA over a range of charge ratios as indicated in Figure 5. The concentration of plasmid DNA during complex formation remained constant at 2.5 μg/mL, while the concentration of the nanotubes ranged from 8.25 to 150 μg/mL, depending upon the type of tube and the charge ratio examined. In all three cases, f-CNTs are clearly able to compact DNA. SWNT-NH_3^+ (Figure 5A) appear the least efficient in compacting DNA. At a charge ratio of 1:1, only 43% of DNA is condensed, gradually increasing to 58% at 6:1. Little to no further condensation appears to occur at higher charge ratios. Strikingly, more than 96% of DNA is condensed by MWNT-NH_3^+ **2** (Figure 5C) at a charge ratio of 1:1 and 99% of DNA is condensed at a charge ratio of 6:1 and above. In the case of SWNT-Lys-NH_3^+ **3** (Figure 5B) which, as indicated in Table 1, have a similar surface charge load as MWNT-NH_3^+, approximately 74% of DNA appears condensed at a 1:1 charge ratio, gradually increasing to 85% at 6:1, reaching

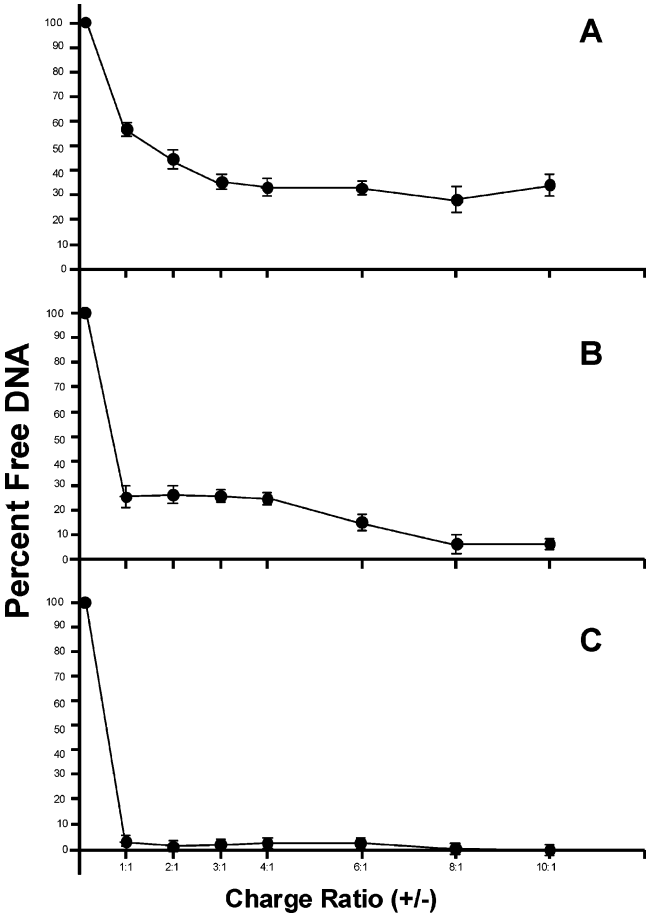

Figure 5. DNA condensation following complexation with functionalized carbon nanotubes. Condensation of 2.5 μg/mL DNA complexed to f-CNTs at various charge ratios expressed as a percent of PicoGreen fluorescence of 2.5 μg/mL free DNA: (A) SWNT-NH_3^+:DNA; (B) SWNT-Lys-NH_3^+:DNA; (C) MWNT-NH_3^+:DNA.

maximum condensation at 10:1, where more than 92% of DNA is condensed.

The PicoGreen data confirm the observation of the apparently less dense packing of the DNA following interaction with the SWNT-NH_3^+ compared to the MWNT-NH_3^+ as seen in the SEM images (Figure 2), and the lack of a detectable increase in the SWNT-NH_3^+ RU signal by SPR (Table 1). This is thought to be due to the lower charge loading efficiency and the relatively restricted access to the positive charges available on the SWNT-NH_3^+ when compared to the other types of f-CNT. Likewise, the MWNT-NH_3^+ appear to condense DNA most efficiently.

Next, we studied the migration of the f-CNT:DNA complexes by agarose gel electrophoresis and the degree of DNA condensation by EtBr (ethidium bromide) exclusion (Figure 6). The plasmid pCMV−βgal used in these studies was highly purified such that approximately 85% was supercoiled with the remaining 15% in an open circular form (lane 1, Figure 6A). The condensation of DNA by f-CNT excludes EtBr intercalation, quenching the fluorescence signal. Therefore, it was not possible to observe condensed DNA participating in the f-CNT:DNA complexes. In general, the fluorescent bands observed in Figure 6 originate from free (uncomplexed) DNA which allows for adequate EtBr intercalation.[28] Figure 6 also reveals an overall decrease in the fluorescence intensity of the free DNA bands with increasing f-CNT:DNA charge ratio, due to reduced

(31) Tsai, J. T.; Furstoss, K. J.; Michnick, T.; Sloane, D. L.; Paul, R. W. *Biotechnol. Appl. Biochem.* **2002**, *36*, 13−20.

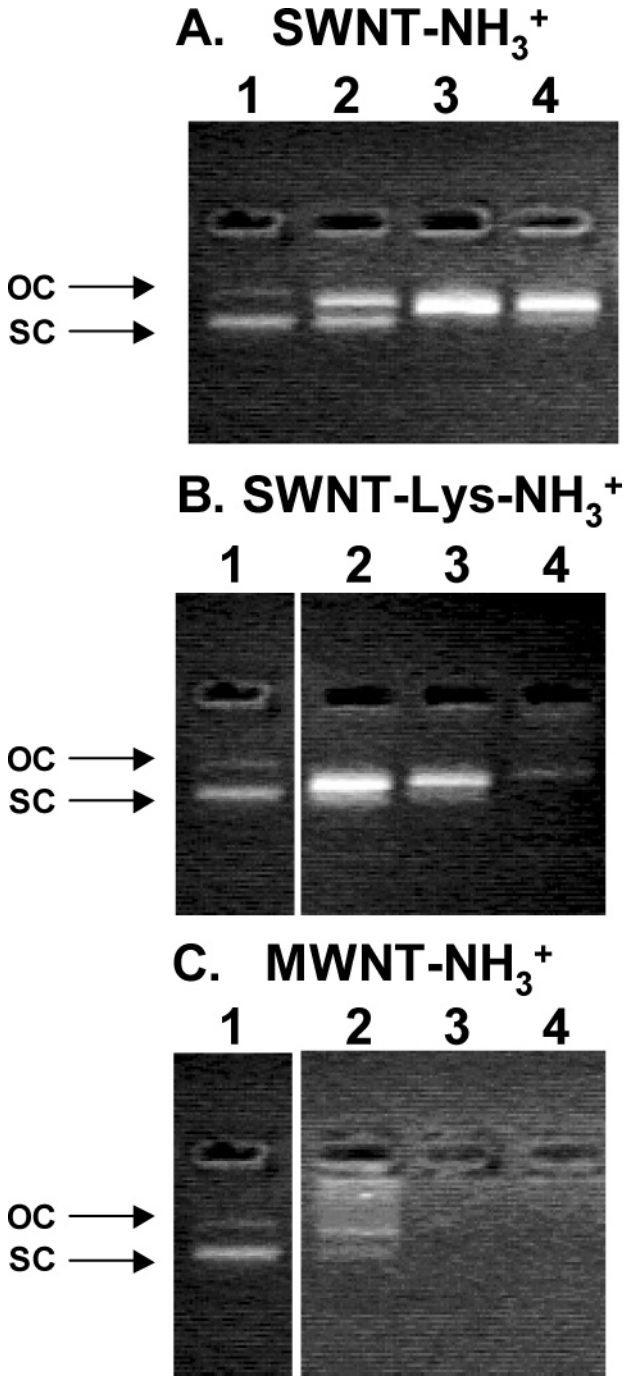

Figure 6. Electrophoretic motility of f-CNT:DNA complexes. In all panels, lane 1 represents 0.2 μg of free DNA. All other lanes contain f-CNT complexed to 0.2 μg of DNA at various ± charge ratios: lane 2, 1:1; lane 3, 6:1; lane 4, 10:1. OC = open circular; SC = supercoiled.

availability of DNA bases for EtBr intercalation caused by the higher degree of DNA condensation. Typically, this assay is used to study the migration of different types of DNA conformations as indicated by a shift in their migration rate. In our case, this was possible only in the case of SWNT-NH_3 (Figure 6A), which does not seem to be able to fully condense DNA. In lanes 2−4 different conformations of free DNA were evident, which can include nicked DNA.

We also found that the data in Figure 6 are in striking agreement with the previous experiments. In the case of SWNT-NH_3^+:DNA, a strong fluorescent signal is observed in lane 2,

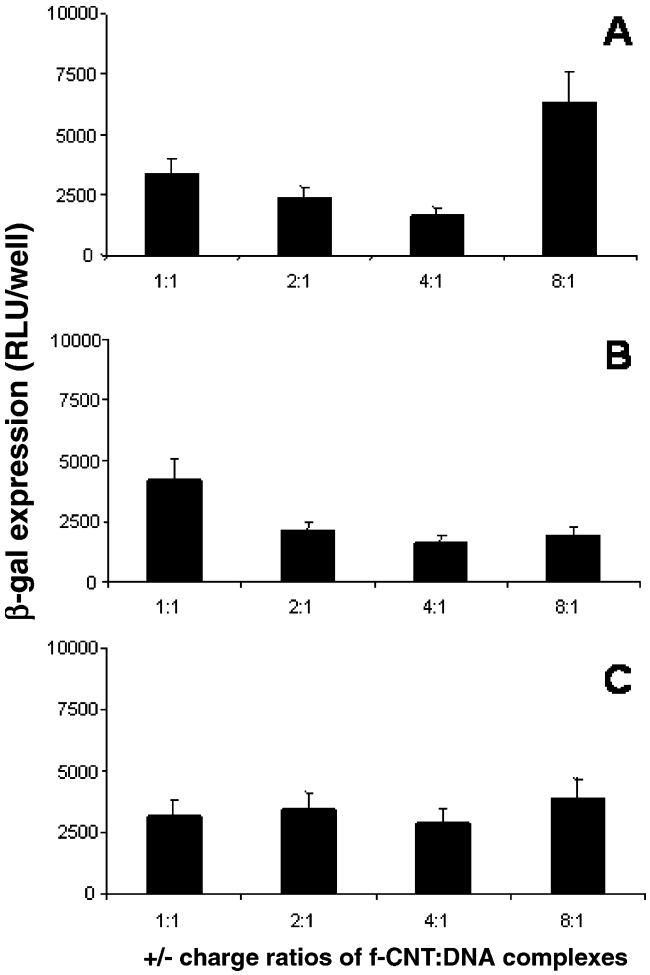

Figure 7. Expression of β-gal marker gene in human lung carcinoma cells (A549) following gene delivery with f-CNT:pDNA complexes at various charge ratios: (A) SWNT-NH_3^+:DNA; (B) SWNT-Lys-NH_3^+:DNA; (C) MWNT-NH_3^+:DNA (gene expression levels shown above DNA control in the absence of CNT using luminometry assay).

corresponding to the 1:1 charge ratio (Figure 6A), indicating the presence of a large amount of free DNA. There is a strong decrease in the fluorescence intensity and an increase in the upward shift of the free DNA bands as the charge ratio is increased to 6:1, but little difference is observed when the ± charge ratio is further increased to 10:1. This is expected as the PicoGreen data indicated that the amount of complexed DNA reaches a plateau at this range (see also Figure 5A). Complexation between **3** and DNA (Figure 6B) is stronger as observed by the overall weaker fluorescence intensity of the free DNA bands when compared to those of the SWNT-NH_3^+:DNA, and the gradual disappearance of fluorescence with increasing charge ratios, indicating even further reduction in the amount of free DNA available for intercalation. In the case of **2**, we can only see a faint fluorescent signal at the 1:1 charge ratio due to the very small amounts of free DNA present (lane 2, Figure 6C; see also Figure 5C). In the same lane we believe the faint smear detected is due to DNA that interacts with **2** but is not fully condensed, allowing for some EtBr intercalation, also indicating the wide mass distribution of these complexes. For higher MWNT-NH_3^+:DNA ratios the fluorescence band disappears since the entire amount of DNA is fully condensed.

Although there appears to be an upward shift in the location of the free DNA band when f-CNT are present in the gel, this

is most likely caused by alteration of the running buffer due to the high ionic strength of the nanotubes themselves. While it is possible that this shift may be due to nicking of the supercoiled DNA, either due to interaction with nanotubes or sustained during the mixing process, causing the DNA to relax to a more open form, control studies in which high concentrations of **1** alone (12 mg/mL) were run in blue-green loading buffer demonstrated a clear retardation of the dye's movement, indicating that the ionic strength of the running buffer can be responsible for changes in the migration of molecules in the gel.

Finally, we looked at the gene-transfer efficiency of the various f-CNT:DNA complexes formed. The data demonstrate that all three types of complexes are able to transfect A549 cells with greater efficiency than naked DNA, which was normalized to a zero value in all three figures (Figure 7A−C). SWNT-NH_3^+ appear to be most efficient at gene transfer when complexed to DNA at an 8:1 charge ratio, while SWNT-Lys-NH_3^+ appear most efficient at a 1:1 charge ratio. Interestingly, the PicoGreen data indicate that, at these charge ratios, approximately 30% of DNA is free to interact with the dye in the case of **1**, and a strikingly similar 25% of DNA is free in the case of **3**. Not surprisingly, in the case of **2**, since even at very low charge ratios DNA is fully condensed, there does not appear to be much difference in their transfection efficiency across all charge ratios and DNA dose studied. It is important to note that while the transfection efficiency of **3**, which at high charge ratios condensed 95% of DNA, appears to decrease with increasing charge ratio, the same effect is not found with **2** group, which, as noted, maintains similar levels of transfection efficiency across all charge ratios. This may be an indication that the structure of the multiwalled nanotubes, which are both longer and wider than the single-walled tubes, may also be playing a critical role.

Discussion

This report characterizes the physicochemical interactions between cationically functionalized carbon nanotubes and DNA, building the foundation for the construction of novel, carbon nanotube-based gene-transfer vector systems. Though other groups have studied the interaction of carbon nanotubes with DNA, in general, these investigations were focused on using single-stranded DNA (ssDNA) to increase the solubility and reduce the polydispersity of nanotubes in aqueous solutions, allowing the formation of nanoassemblies useful as molecular probes or in nanoelectroctronics applications. For example, Zheng et al. demonstrated that SWNTs have an affinity for single-stranded DNA, presumably by hydrophobic interactions,[19,32] and Williams et al. demonstrated that CNTs functionalized with PNA specifically bind DNA containing a complementary sequence.[13] Additionally, carbon nanotubes have been functionalized directly with DNA,[33] allowing the nanotubes to be directed into a nanoassembly by DNA−DNA interactions. However, in no case has the potential of using CNTs to condense plasmid DNA as gene-transfer vectors been previously exploited.

We observed that CNTs possess many characteristics that make them desirable as gene delivery vectors. They are readily produced, are stable for long-term storage, are soluble in aqueous solution, have low toxicity in vitro,[22,25] and can be functionalized with numerous cationic groups at various densities to tailor their use for gene delivery applications. However, prior to being studied as gene therapeutic agents, principles of rational design, in particular, optimization of charge ratio and structural characterization, must be applied for the development of nanotube−DNA gene delivery systems.[34]

Most cation− and polycation−DNA complexes will transfect in vitro and in vivo at a variety of charge ratios, though transfection efficiency greatly is increased when the charge ratio is optimized. A variety of factors, including complex size, surface charge, DNA topology, and degree of condensation, play a role in determining which charge ratio will be optimal for gene transfer.[35] In order for f-CNT:DNA complexes to be useful for gene delivery, plasmid DNA must be condensed by the nanotube, carried into the target cell, intracellularly detach from the nanotube, and enter the nucleus prior to transgene expression. Therefore, it is important to study the physical state of DNA when bound to CNT. The SEM data of f-CNT:DNA complexes clearly show the formation of a supramolecular lattice, with parallel bundles of nanotubes forming a framework to which condensed packets of DNA adhere (Figure 2). Most interestingly, the DNA complexed to the MWNT appears to be more tightly associated with the nanotubes than when complexed to SWNT. This may be an important consideration for using these complexes for gene transfer, particularly in vivo, as highly condensed DNA is more resistant to serum inhibition.[36] However, if DNA is too tightly complexed, it may be unable to detach from the nanotube, therefore leading to compromised gene expression. It is important to note that the supramolecular f-CNT:DNA complex SEM samples are not representative of the complex structure in solution, due to the drying process necessary to obtain the imaged samples. Nevertheless, valuable comparative observations indicated differences in the DNA condensation patterns occurring in f-MWNT:DNA and f-SWNT:DNA complexes.

To confirm the observation from the SEM studies that DNA appears to bind to f-MWNT more tightly than f-SWNT in an aqueous solution, we quantified the interactions using SPR (Figure 4) by covalently binding the nanotubes onto a gold sensor chip and injecting an aqueous solution containing the plasmid DNA. Because of the difference in the charge loading between **1** and **2**, we incorporated a second type of f-SWNT into this experiment, namely, **3**. The MWNT-NH_3^+ have approximately twice as many positive charges per unit mass as the SWNT-NH_3^+ but have a functional group density similar to the SWNT-Lys-NH_3^+ (Table 1). By comparing the SPR results of **1** to those of **3**, we could assess the effect of increasing charge density while maintaining a constant surface area, and conversely, comparing **3** to **2**, we were able to assess the effect of changes in surface area while maintaining a constant charge density.

(32) (a) Zheng, M.; Jagota, A.; Strano, M. S.; Santos, A. P.; Barone, P.; Chou, S. G.; Diner, B. A.; Dresselhaus, M. S.; McLean, R. S.; Onoa, G. B.; Samsonidze, G. G.; Semke, E. D.; Usrey, M.; Walls, D. J. *Science* **2003**, *302*, 1545−1548. (b) Strano, M. S.; Zheng, M.; Jagota, A.; Onoa, G. B.; Heller, D. A.; Barone, P.; Usrey, M. *Nano Lett.* **2004**, *4*, 543−550.

(33) Dwyer, C.; Guthold, M.; Falvo, M.; Washburn, S.; Superfine, R.; Erie, D. *Nanotechnology* **2002**, *13*, 601−604.

(34) Kostarelos, K. *Adv. Colloid Interface Sci.* **2003**, *106*, 147−168.

(35) (a) Congiu, A.; Pozzi, D.; Esposito, C.; Castellano, C.; Mossa, G. *Colloids Surf., B* **2004**, *36*, 43−48. (b) Ryhanen, S. J.; Saily, M. J.; Paukku, T.; Borocci, S.; Mancini, G.; Holopainen, J. M.; Kinnunen, P. K. *Biophys. J.* **2003**, *84*, 578−587. (c) Simberg, D.; Danino, D.; Talmon, Y.; Minsky, A.; Ferrari, M. E.; Wheeler, C. J.; Barenholz, Y. *J. Biol. Chem.* **2001**, *276*, 47453−47459.

(36) Houk, B. E.; Hochhaus, G.; Hughes, J. A. *PharmSci* **1999**, *1*, U1−U9.

Interestingly, while we could link all three types of nanotubes to the sensor chips, we were only able to see a shift in the sensorgram following the introduction of DNA for SWNT-Lys-NH_3^+ and MWNT-NH_3^+, indicating that the SWNT-NH_3^+:DNA interactions are significantly weaker than those of SWNT-Lys-NH_3^+ and MWNT-NH_3^+. In addition, the MWNT-NH_3^+ were able to bind significantly more DNA than the SWNT-Lys-NH_3^+. It is clear that the measured interactions are primarily electrostatic and not of hydrophobic nature, as demonstrated by the following: (a) the lack of binding to the SWNT-NH_3^+, which upon immobilization maintains its hydrophobic properties but loses most of its cationic charges, and (b) the complete dissociation of the complex following exposure to $MgCl_2$.

The conclusions from the SPR study that MWNT-NH_3^+ were able to bind significantly more DNA than the SWNT-Lys-NH_3^+, and the observation that SWNT-NH_3^+ do not bind DNA as efficiently as the other two types of nanotubes, were strongly supported by the PicoGreen dye exclusion assay data (Figure 5). These data also support the observation that the MWNT-NH_3^+ compact DNA more tightly than the other two types of nanotubes. The PicoGreen data show a steep drop in the amount of free DNA present in solution following the interactions of DNA and MWNT-NH_3^+, indicating that even, at low charge ratios, most of the DNA is condensed. It is necessary to use an 8-fold excess of SWNT-Lys-NH_3^+ to condense the DNA to an equivalent degree. These data nicely correlate with the BIAcore assay data, since smaller amounts of DNA were condensed by the SWNT-Lys-NH_3^+ in comparison to the MWNT-NH_3^+.

The conformation of the DNA and the efficiency of condensation offered by the f-CNT and the overall motility characteristics of the nanotube:DNA complexes were examined by the mobility shift experiments. However, due to the high degree of condensation of the DNA caused by interaction with the f-CNT, EtBr was excluded from the condensed plasmid DNA, making it impossible to directly monitor the migration of an f-CNT:DNA complex. However, by hypothesizing that the DNA that was visible on the gel corresponded to free DNA rather than DNA involved in forming the f-CNT complex, we were able to indirectly monitor the formation of the complex. As greater amounts of DNA are condensed, the amount of free DNA, and therefore the corresponding fluorescence signal, will be reduced. The data from the PicoGreen assay and SPR analysis indicated that, with increasing $\pm$ charge ratios, greater amounts of DNA are condensed, with MWNT-NH_3^+ able to most efficiently condense DNA, followed by SWNT-Lys-NH_3^+ and SWNT-NH_3^+. Indeed, this is exactly what the gel images demonstrated as the fluorescence intensity in both the MWNT-NH_3^+ and SWNT-Lys-NH_3^+ lanes rapidly declined with increasing charge ratio, indicating the formation of tightly packed complexes with the DNA, as observed with all previous experimental techniques. In fine agreement with the PicoGreen data, which also indicated that SWNT-NH_3^+ were forming weak DNA complexes even at high charge ratios, the gel images indicate that large amounts of free DNA are present even at the 10:1 ($\pm$) charge ratio.

Very interestingly, our initial in vitro gene delivery and expression studies indicated that SWNT-NH_3^+:DNA complexes were able to upregulate gene expression.[25] We repeated those studies herein using a different mammalian cell line (human lung carcinoma, A549) and incorporating two new types of f-CNT to demonstrate that all three types of carbon nanotubes are able to mediate enhanced gene transfer over plasmid DNA alone (Figure 7). While these systems will need much further work to develop to their full potential, the data suggest that optimal gene-transfer efficiency when using f-CNT:DNA complexes may occur when DNA is only partially condensed, and that MWNT-NH_3^+, which are able to transfect cells even with a high degree of DNA condensation, may offer an advantage over f-SWNT. Determination of optimal transfection conditions and the mechanism of cell entry, as well as the roles that charge density and nanotube length and width play on transfection efficiency require further studies to elucidate. However, the present data clearly demonstrate that f-CNT designed with specific characteristics such as high or low surface charge density and single-walled or multiwalled structure, interact with DNA differently, leading to various supramolecular structures. As this study shows, provided that those differences can be measured and monitored, correlations with gene delivery efficiencies can start to be drawn, with the potential for development of f-CNT-based transfection agents. In view of longer term pharmacological applications of such nanotube:DNA systems, a degree of strong electrostatic interaction is necessary to avoid dissociation on dilution or competition with other molecular species (e.g. blood components) interacting with the complex. It is very likely that determination of a fine balance between DNA condensation, tight association with the f-CNT surfaces, and intravascular and intracellular DNA release will determine their capacity as novel gene delivery systems.

In conclusion, the present study indicates that both f-CNT surface area, due to differences in both length and width of the nanotubes, and charge density are critical parameters for determining the interaction and electrostatic complex formation between f-CNT with DNA. The large surface area of the MWNT-NH_3^+ allows more DNA to tightly associate. Currently we know that SWNT-NH_3^+:DNA complexes are capable of transfecting cells in vitro, and this report demonstrates that both SWNT-Lys-NH_3^+ and MWNT-NH_3^+ can also achieve that at varying degrees of efficiency. Correlation of the current observations with future gene expression studies will allow the implementation of rational design strategies in the development of f-CNT:DNA complexes as effective gene delivery vector systems.

Acknowledgment. This work was financially supported by the CNRS, the University of Trieste, and MIUR (PRIN 2004, prot. 2004035502). Ken A. Smith from Carbon Nanotechnologies, Inc., is also greatly acknowledged for the generous gift of carbon nanotubes.

Supporting Information Available: SEM images and PicoGreen data of f-CNT alone (PDF). This material is available free of charge via the Internet at http://pubs.acs.org.

JA0441561